Research and test of the measurement sensing device for the downforce of no-till planter row unit gauge wheels

Jiajie Shang[1], Liyi Liu[1], Ruifeng Zhang[1], Hongcheng Li[1],
Shouyin Hou[1], Hongxin Liu[1,2*], Haitao Chen[1]

(1. *College of Engineering, Northeast Agricultural University, Harbin 150036, China*;
2. *College of Mechanical and Electrical Engineering, Suqian University, Suqian 223800, Jiangsu, China*)

Abstract: To effectively obtain the downforce of the gauge wheels in real time, mechanical models of the interaction among the ground, gauge wheels, gauge wheel arms, and depth adjustment lever were constructed. A measuring method was proposed for monitoring the downforce through a two-dimensional radial sensing device, and a corresponding prototype was designed. Through simulation analysis of the sensing device with ANSYS, a 45° angle was determined to exist between the strain gauge axis and the sensing device axis, and the Wheatstone bridging circuit of R1+R3−R5−R7 (R stands for resistance strain gauge, different figures represent the strain gauge number) and R2+R4−R6−R8 was adopted. According to performance and calibration tests for the sensing device, the maximum interaction effect between the X and Y axes was 2.52%, and the output signal was stable and consistent. The standard error of the slope of the fitting equation of the downforce calculation model is 0.008. According to the field test, the average downforce of the gauge wheels was 1148, 1017, 843, and 713 N, at different sowing speeds of 6, 8, 10, and 12 km/h, respectively. The coefficients of variation were 0.40, 0.41, 0.62, and 0.71, respectively. The results indicate that the downforce fluctuation of the gauge wheels became more severe with increasing planting speed. Both the strain simulation analysis and field test verified that the measurement method is accurate and reliable, the performance of the sensing device is stable, the measurement method and sensing device meet the application requirements and lay a foundation for the research of accurate and stable control of downforce of no-till planter.
Keywords: no-till planter, gauge wheel downforce, two-dimensional radial force sensing device, strain analysis, measurement mode and method

1   Introduction

With the development of modern agricultural science and technology, precision seeding technology is developing with intelligent automation[1-4]. Especially considering no-tillage sowing under poor sowing conditions, the significance of sowing downforce on effective control is prominent, because precise sowing downforce plays an important role in achieving a reliable germination rate and strong plant emergence[5-7]. If excessive downforce is applied, especially in soft or moist soils, the soil may be overly compacted which can affect the ability to germinate seeds to break. If insufficient downforce is applied, particularly in hard or

dry soil, the planter may ride up and out of the soil, resulting in an insufficient depth of the furrow and affecting the germination rate[8-11]. As the gauge wheels are the main component bearing the downforce of the planter row unit, it is very important to obtain data on gauge wheel downforce. This is applied as a premise to realize accurate control of sowing depth through active mode monitoring[12,13].

There are many studies on intelligent monitoring and control of precision seeding[14-16] and precision fertilization[17-20] of planters, but there are relatively few studies on monitoring the downforce of the gauge wheels. Existing reports mainly include Huang et al.[21], Zhu et al.[22], and Jia et al.[23] used a PVDF (polyvinylidene fluoride) piezoelectric film and flex bending sensor pasted on a rubber gauge wheel and calculated the downforce by converting the deformation of the gauge wheel surface into a voltage signal during planting. This scheme is feasible but presents a problem of lagging data. Li et al. hinged a pressure sensor, which was installed above the covering roller, and adjusted the amount of overburden by collecting the downforce of the covering roller[24], but could not provide an effective basis for consistent control of sowing depth. At present, the general installation position of the downforce sensing device should be the depth adjustment lever, gauge wheel arm, or hinged position. For example, Lynn et al. installed a gauge wheels downforce sensing device on the depth adjustment lever[25]. Jing et al.[26] and Paul et al.[27] replaced the depth adjustment lever connection pin with a downforce sensor. Precision Planting LLC installed a downforce sensing device on gauge wheel arms[28]. Bai et al.[29] and Fu et al.[30] used a shaft pin sensor (instead of the limit pin shaft) as the downforce sensor and hinged this sensor synchronously

with the depth limit block. By measuring the force between the gauge wheels and the depth limit block as the downforce, their scheme obtained data in a timely and accurate manner. However, under different sowing depth control conditions, the gauge wheel downforce obtained was different, resulting in a problem of large deviation of measurement accuracy under different sowing depths. To compensate for the above problems, Gao et al.[31] developed a real-time monitoring device on the gauge wheel downforce and a monitoring method that adopted force and angle sensors to correct the original downforce model and obtain more accurate gauge wheel downforce data. However, the scheme required two different types of sensors simultaneously monitoring the planter row unit, which made the device more complicated.

To sum up, real-time, effective, and accurate monitoring of the downforce of gauge wheels is the premise and basis of the research on accurate and stable control of no-till planter sowing depth. Therefore, it is necessary to research a set of effective measurement methods and accurate sensing devices to achieve real-time and effective downforce for gauge wheels. The purpose of this study was to propose a new measurement method, that is, a set of two-dimensional radial sensing devices used to monitor both X and Y forces. Then the downforce of gauge wheels and the position of the sowing depth adjustment gear can be obtained through the corresponding mathematical model conversion, and the angle sensing device is omitted, so the sowing depth monitoring device is simplified.

2   Materials and methods

2.1   Structure and principle of the electrohydraulic profiling row unit

2.1.1   Structure

The research object is a 2BMG-2 tractive no-tillage precision planter. The structural schematic diagram of the electrohydraulic profiling row unit is shown in Figure 1. It is mainly composed of a no-till colter, row cleaners, gauge wheels, closing wheels, double parallel arm, hydraulic cylinder, proportional pressure regulator, etc. Its operating width is 1.3 m (adjustable range 0.8-1.4 m) and its sowing depth adjustment range is 30-80 mm.

2.1.2   Working principle

The electrohydraulic profiling row unit of the planter can realize the automatic control of seeding depth by collecting and monitoring the downforce of gauge wheels obtained by the designed sensing device in real-time.

The specific working principle is as follows: Firstly, the designed load-sensing device monitors the downforce of the gauge wheels and feeds back to the measurement and control unit. Secondly, the measurement and control unit adjusts the double-acting hydraulic cylinder through the oil pressure controller and the proportional pressure regulator and then realizes the reciprocating movement of the hydraulic rod by adjusting the oil pressure in the rodless chamber of the hydraulic cylinder. Thus, the downforce of the row unit and the depth of ditching can be adjusted, so as to obtain a more suitable sowing depth.

The control system adopts an inner and outer double loop structure, which further improves the control precision and system response speed.

2.2   Establishment and analysis of the mechanical model

As shown in Figure 2, the gauge wheels, gauge wheel arm, and depth adjustment lever are installed on the row unit of the planter. The gauge wheel is installed on the lower end of its gauge wheel arm, and the upper end of the gauge wheel arm is hinged on the
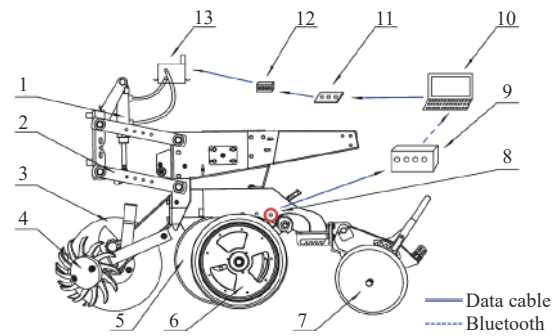
1. Hydraulic cylinder 2. Parallel four-bar profiling mechanism 3. No-till coulter 4. Row Cleaner 5. Disc opener 6. Gauge wheels 7. Closing wheels 8. Downforce sensor of gauge wheels 9. Data acquisition device 10. Computer 11. Single-chip controller 12. Hydraulic controller 13. Proportional pressure regulator

a. Structural representation of the 2BMG-2 electrohydraulic profiling row unit

1. Proportional pressure regulator 2. Hydraulic cylinder 3. Parallel four-bar mechanism

b. Prototype of electro-hydraulic profiling control device

Figure 1   Structural of the 2BMG-2 electrohydraulic profiling row unit of planter

a. Installation position on the prototype   b. Installation drawing with a cutaway view
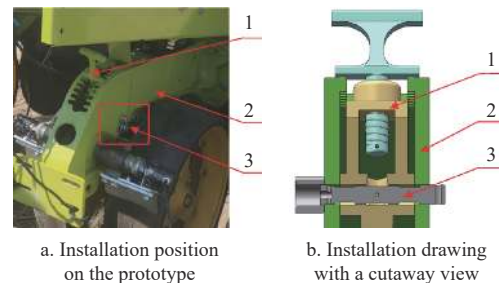
1. Depth adjustment lever 2. Rack of row unit 3. two-dimensional radial sensor

Figure 2   Installation position schematic diagram of the sensing device

frame. The upper part of the depth adjustment lever is the adjusting handle, which is used to adjust the sowing depth.

The bearing condition determines the measuring range and placement form of the downforce sensing device. In this downforce measuring device, the original depth adjustment groove pin between the depth adjustment lever and frame should be replaced with the designed two-dimensional radial sensing device. Moreover, the sensing device and the depth adjustment lever should be fixed with a pin to allow them to rotate synchronously. The installation position of the sensing device is shown in Figure 2.

2.2.1   Force analysis of the depth adjustment lever and gauge wheel arm

The relative position and force analysis diagram describing the depth adjustment lever and gauge wheel arm is shown in Figure 3. It should be noted that point B is a simple contact between the gauge wheel arm and the depth adjustment lever.
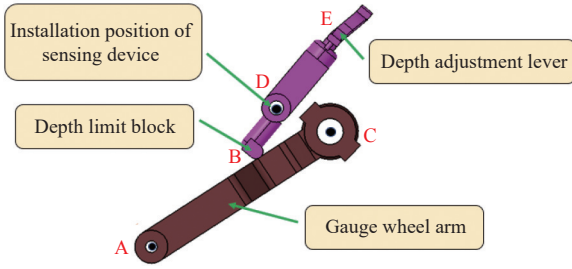
Note: Point A represents the hinge point between the gauge wheel and the gauge wheel arm; Point B represents the contact point between the depth limit block and the gauge wheel arm; Point C represents the hinged point between the gauge wheel arm and the frame of row unit. Point D represents 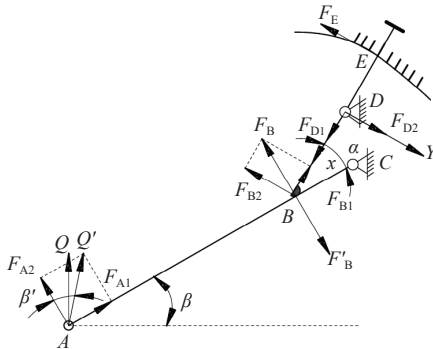the downforce sensor installation position; Point E represents the contact point between the depth adjustment lever and the frame of row unit.

a. Diagram of relative position

Note: Points A, B, C, D, and E are noted as Figure a; Q denotes the downforce of gauge wheels, N; Q' stands for constraint reaction from the ground to the gauge wheel; F_{A1}, parallel to the AC rod, is the component force of Q', N; F_{A2}, perpendicular to the AC rod, is the component force of Q', N; β denotes the angle between the gauge wheel and ground; β' denotes the angle between the force of F_{A2} and the force of Q'; F_B and F'_B are a pair of forces and reactions acting on point B, respectively; F_{B1}, parallel to the BE rod, is the component of F_B, N; F_{B2}, perpendicular to the BE rod, is the component of F_B, N; F_{D1}, parallel to the BE rod, is the X-direction force measured by the sensing device, N; F_{D2}, perpendicular to the BE rod, is the Y-direction force measured by the sensing device, N; F_E is the force of the frame of row unit on the depth adjustment lever.

b. Schematic diagram of force analysis

Figure 3　Relative position and force analysis diagram of depth adjustment lever and gauge wheel arm

The force analysis on the depth adjustment lever BE can be obtained by

$$\begin{cases} F_{B2} + F_E - F_{D2} = 0 \\ -F_{B2}l_{BD} + F_E l_{DE} = 0 \\ l_{BD} + l_{ED} = l_{BE} \end{cases} \tag{1}$$

From the derivation of Equation (1), the force F_{B2} is

$$F_{B2} = \frac{F_{D2}l_{DE}}{l_{BE}} \tag{2}$$

where, F_{B2}, perpendicular to the BE rod, is the downforce of gauge wheels, N; F_E, perpendicular to the BE rod, is the force of the frame on the depth adjustment lever, N; F_{D2}, perpendicular to the BE rod, is the Y-direction force measured by the sensing device, N; l_{BD} is the length of BD, mm; l_{DE} is the length of the DE, mm; l_{BE} is the length of the BE, mm.

In addition:

$$\begin{cases} F_B = \sqrt{F_{B1}^2 + F_{B2}^2} \\ F'_B = F_B \\ F_{B1} = F_{D1} \end{cases} \tag{3}$$

where, F_{B1}, parallel to the BE rod, is the component of F_B, N; F_B, perpendicular to the AC rod, is the force of the gauge wheel arm on the depth adjustment lever, N; F_{D1}, parallel to the BE rod, is the X-direction force measured by the sensing device, N.

The force analysis on the gauge wheel arm AC can be obtained by

$$-F_{A2}l_{AC} + F'_B l_{BC} = 0 \tag{4}$$

From the derivation of Equations (3) and (4), the force F_{A2} is

$$F_{A2} = \sqrt{F_{D1}^2 + \left(\frac{F_{D2}l_{DE}}{l_{BE}}\right)^2} \frac{l_{BC}}{l_{AC}} \tag{5}$$

where, F_{A2}, perpendicular to the AC rod, is the component force of Q', N; l_{BC} is the length of the BC, mm; l_{AC} is the length of the AC, mm.

Then,

$$Q \approx Q' = \frac{\sqrt{F_{D1}^2 + \left(\frac{F_{D2}l_{DE}}{l_{BE}}\right)^2} \frac{l_{BC}}{l_{AC}}}{\cos(\beta')} \tag{6}$$

where, Q denotes the downforce of gauge wheels, N; β' denotes the angle between the force of F_{A2} and the force of Q'.

For the selected 2BMG-2 no-till planter row unit, l_{DE}=116 mm, l_{BE}=166 mm, l_{AC}=248 mm, and l_{BC} will be different under different sowing depth adjustment gear, and its maximum value is 106.6 mm. In addition, the angle between F_{A2} and Q' is small (the maximum value is 5.11°). Here, F_{A2} can be approximately assigned 2000 N to estimate the measuring range. By substituting relevant values into Equation (5), it can be obtained that the maximum value of F_{D1} is 6012.12 N and that of F_{D2} is 8603.38 N. Considering the working conditions of a no-tillage planter, herein, both the X- and Y-direction measuring range of the designed sensing device is determined to be 10 000 N.

2.2.2　Analysis of the two-dimensional force relationship of the sensing device

As shown in Figure 3b, the forces F_{D1} and F_{D2} can be expressed as,

$$\begin{cases} F_{D1} = F_{B1} = F_B \sin\alpha \\ F_{D2} = \frac{F_{B2}l_{BE}}{l_{DE}} = \frac{F_B \cos\alpha l_{BE}}{l_{DE}} \end{cases} \tag{7}$$

From Equation (7), it can be deduced that the two-direction force relationship of the sensing device is

$$\frac{F_{D1}}{F_{D2}} = \tan\alpha \frac{l_{DE}}{l_{BE}} \tag{8}$$

where, α is the angle between the depth adjustment lever and the gauge wheel arm, (°).

For a definite no-tillage planter, l_{DE} and l_{BE} are determined. According to Equation (8), the ratio of the two-direction force measured by the sensing device is only related to the angle between the depth adjustment lever and the gauge wheel arm. Therefore, in practical applications, the position of the depth adjustment lever can be determined by the ratio of this two-dimensional force.

2.2.3　Force analysis of the gauge wheels

The force of the gauge wheel arms mainly comes from the force of the ground in contact with the gauge wheels. Therefore, it is necessary to analyze this force of the gauge wheels. During this analysis, the wheels were assumed to be a rigid component because they operate on soft ground. The relevant mechanical model is shown in Figure 4.
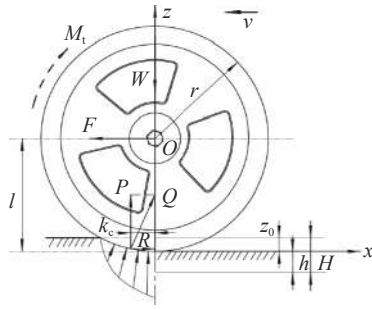
Note: F is the horizontal traction force on the gauge wheels, N; W is the vertical load (including self-gravity) on the gauge wheels, N; M_t is the drag torque, N·m; Q is the force from ground on the gauge wheels, N; P is the vertical component of ground force Q, N; R is the horizontal component of ground force Q, N; l is the distance between the center of gauge wheels and ground, mm; k_c is ground force offset, mm; r is radius of the gauge wheels, mm; Z_0 is sinking depth of gauge wheels, mm; H is ditching depth, mm; h is the depth of seed to surface, mm.

Figure 4   Force analysis diagram for gauge wheels

It is assumed that when the gauge wheels with uniform speed of rotation. Then, the force equilibrium equation can be formulated as follows:

$$\begin{cases} \sum F_x = F - R = 0 \\ \sum F_z = W - P = 0 \\ \sum M_0 = Rl - Pk_c - M_t = 0 \end{cases} \tag{9}$$

where, F is the horizontal traction force on the gauge wheels, N; W is the vertical load (including self-gravity) on the gauge wheels, N; M_t is the drag torque on the gauge wheels, N·m; Q is the force from the ground on the gauge wheels, N; P is the vertical component of ground force Q, N; R is the horizontal component of ground force Q, N; l is the distance between the center of gauge wheels and ground, mm; k_c is the ground force offset, mm; r is the radius of the gauge wheels, mm; Z_0 is sinking depth of gauge wheels, mm; H is the ditching depth, mm; h is the depth of seed to surface, mm.

The analysis shows that R, l, and k_c are variables generated due to the horizontal traction force F. When there is no traction force, then $R=0$, $k_c=0$ and $l=r$. When the traction force increases, R, l, and k_c all change with F. Herein the maximum value of R is denoted as $R_{max}=frW$, where fr is the rolling friction coefficient. The values of l and k_c are related to the structure of the gauge wheels, the load, and the soil properties. In addition, if the value of k_c is small, assume that P is equal to Q. Therefore, assume that the downforce of the gauge wheels is equal and opposite to the resultant force Q of the ground.

2.3   Design of the sensing device
2.3.1   Structure
According to the force analysis of the sensing device and considering the structure and actual size of the no-tillage planter row unit, the designed two-dimensional radial sensing device structure is shown in Figure 5. A through pin hole is arranged at the small head of the sensing device to install a fastening pin shaft, which is used to limit the axial device movement. On the surface of the device, the left and right ring grooves are manufactured along the circumferential direction. A radial lead hole is provided near the large head. Wire slots are machined along both sides of the sensing device in the axial direction. The hole of the radial lead wire is

connected to the bus hole at the large head so that the wire of the measuring bridge (composed of the strain gauge) passes through the bus hole and connects to the data acquisition device.
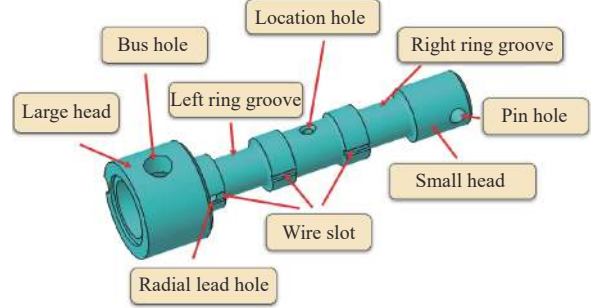

Figure 5   Structure sketch of the sensing device

According to the size and application condition of the sensing device, its strength was verified. Two shear planes were generated when the sensing device was applied, which is referred to as the double shear configuration[32].

The shear strength verified of the sensing device is as follows:

$$\tau = \frac{P}{2A} \tag{10}$$

where, τ is the shear strength of the sensing device, MPa; P is the load on the sensing device, N; A is the cross-sectional area of the sensing device, mm².

The security coefficient was 1.5, the load of the sensing device was 15 000 N, and the cross-sectional area of the sensing device was 113.04 mm². Therefore, 66.35 MPa can be calculated by Equation (10). It was far less than the allowable shear stress, so the shaft pin sensor met the application requirements.

2.3.2   Strain simulation analysis
To obtain a reasonable strain gauge arrangement scheme (including arrangement angle and bridge mode) for the sensing device. Strain simulation analysis was carried out with ANSYS software Version 19.0 (ANSYS Corporation, Pittsburgh, Pennsylvania, USA).

1) Model establishment

The material of the sensing device is selected 17-4PH, which has the characteristics of high strength, high hardness, and corrosion resistance, while the residual stress generated by mechanical processing and heat treatment is small, and these excellent material characteristics play a key role in the comprehensive performance and stability of the sensor. The material properties are listed in Table 1[33].

Table 1   Basic material properties

Parameters	Symbol	Value
Elasticity modulus/Pa	E	1.96E+11
Poisson ratio	v	0.3
Density/(kg·m⁻³)	ρ	7750
Yield strength/Pa	σ_s	≥7.90E+08
Tensile strength/Pa	σ_b	≥9.65E+08

Different strain gauges arrangement schemes impose great influence on the performance of the sensing device. Herein, in order to obtain the better strain gauges arrangement angle and bridge mode, two strain gauges arrangement angles and six possible bridging modes placed at angles of 0° and 45° from the axial direction of the sensor were analyzed, as listed in Tables 2 and 3. In addition, the position and distribution of the load may also affect the measurement output. Therefore, five different load distribution

combination forms were simulated at loading positions A and B along the Y-direction, as shown in Figure 6, Tables 2 and 3.

Table 2   Results of the simulation of the strain gauges were located at 0°

Loading position and value/N		R1+R3− R5−R7/	R2+R4− R6−R8/	R1−R3+ R5−R7/	R2−R4+ R6−R8/	R1−R3− R5+R7/	R2−R4− R6+R8/
A	B	$\mu\varepsilon$	$\mu\varepsilon$	$\mu\varepsilon$	$\mu\varepsilon$	$\mu\varepsilon$	$\mu\varepsilon$
10 000	0	143.00	−115.64	454.10	0.13	−1230.30	0.05
7000	3000	57.17	−46.45	500.43	0.12	−717.43	0.01
5000	5000	−0.06	−0.33	531.34	0.12	−375.52	−0.01
3000	7000	−57.28	45.79	562.24	0.12	−33.62	−0.04
0	10 000	−143.11	114.97	608.57	0.11	479.25	−0.07
Average		−0.06	−0.33	531.34	0.12	−375.52	−0.01

Note: 1 $\mu\varepsilon$ = 1×10⁻⁶ ε. ε is the ratio of the change to the original value. Same below.

Table 3   Results of the simulation of the strain gauges were located at 45°

Loading position and value/N		R1+R3− R5−R7/	R2+R4− R6−R8/	R−R3+ R5−R7/	R2−R4+ R6−R8/	R1−R3− R5+R7/	R2−R4− R6+R8/
A	B	$\mu\varepsilon$	$\mu\varepsilon$	$\mu\varepsilon$	$\mu\varepsilon$	$\mu\varepsilon$	$\mu\varepsilon$
10 000	0	9.04	−2274.98	159.00	0.02	−433.48	0.08
7000	3000	3.64	−2281.50	175.19	0.00	−252.09	0.10
5000	5000	0.03	−2285.84	185.98	−0.04	−131.16	0.12
3000	7000	−3.56	−2290.19	196.77	−0.05	−10.23	0.13
0	10 000	−8.97	−2296.71	212.95	−0.07	171.16	0.15
Average		0.04	−2285.84	185.98	−0.03	−131.16	0.12

a. Strain gauge arranged at 0° with the axial

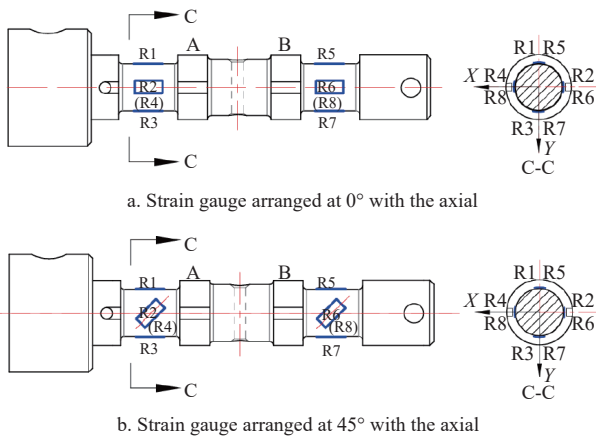b. Strain gauge arranged at 45° with the axial

Figure 6   Schematic diagram of load position and strain gauge arrangement

The strain gauge arrangements are shown in Figure 6. The 8 strain gauges on the sensing device are uniaxial resistance strain gauges, and their arrangement features are as follows: 4 uniaxial strain gauges are laid and applied to each of the left and right patch areas (left and right ring grooves) of the sensing device; R1 to R4 are located on the surface of the left ring groove, and R5 to R8 are located on the surface of the right ring groove. The 4 strain gauges on each ring groove are evenly distributed 90° apart on the circumferent surface and are symmetrical in pairs to the central axis, where R1 and R3 are symmetric, R5 and R7 are symmetric, R2 and R4 are symmetric, and R6 and R8 are symmetric.

2) Simulation results

The simulation results are listed in Table 2 and Table 3.

The performance analysis results of the strain gauges were located at 0°and 45° for the sensor are listed in Table 4 and Table 5, respectively.

3) Analysis of simulation results

According to the analysis of Tables 4 and 5, when the strain gauges were located at 45° along the axial direction of the sensing device, and the bridging mode is R2+R4−R6−R8, the relative error of this loading scheme is small and stable, and its average relative error is 0.27%. At the same time, it has the maximum sensitivity (228 584.40 ε/N) and the minimum cross-sensitivity (0.000 02). Therefore, the sensing device that the strain gauges were located at 45° and the Wheatstone bridging circuit of R1+R3−R5−R7 (R stands for resistance strain gauge) and R2+R4−R6−R8 was adopted finally.

Table 4   Performance analysis results of the strain gauges were located at 0°

Name	R1+R3− R5−R7	R2+R4− R6−R8	R1−R3+ R5−R7	R2−R4+ R6−R8	R1−R3− R5+R7	R2−R4− R6+R8
Sensitivity/ (ε/N)	5.64	33.10	53 133.62	12.00	37 552.26	−1.10
Relative Error/%	141 997.41	19 506.91	8.14	4.47	127.47	308.09
Cross Sensitivity	0.17 045		0.00 023		0.00 003	

Table 5   Performance analysis results of the strain gauges were located at 45°

Name	R1+R3− R5−R7	R2+R4− R6−R8	R1−R3+ R5−R7	R2−R4+ R6−R8	R1−R3− R5+R7	R2−R4− R6+R8
Sensitivity/ (ε/N)	3.69	228 584.40	18 597.69	2.80	13 116.13	11.60
Relative Error/%	13 650.37	0.27	8.12	108.57	129.08	17.93
Cross Sensitivity	0.00 002		0.00 015		0.00 088	

To meet the requirements of measuring two-dimensional orthogonal forces, two groups of Wheatstone bridge circuits are used to measure the X and Y forces[34] and the strain gauges are located at a 45° angle with the axis of the sensing device. Eight uniaxial strain gauges were divided evenly into two groups. The four strain gauges R1 and R3 in the left ring groove and R5 and R7 in the right ring groove were connected to form a full bridge measuring circuit of radial component force in the Y-direction. Four strain gauges R2 and R4 in the left ring groove and R6 and R8 in the right ring groove were connected to form a full bridge measuring circuit of radial component force in the X-direction, as shown in Figure 7. According to the force synthesis principle, the radial resultant force and direction angle are obtained by the downforce measuring sensing device.

a. X direction bridge circuit mode   b. Y direction bridge circuit mode
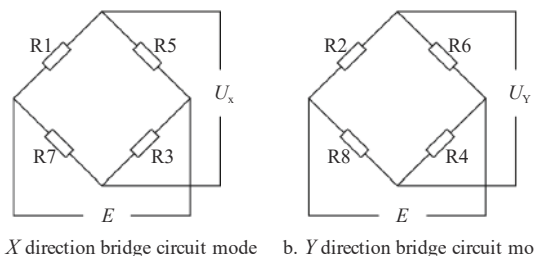
Note: U_x is the output voltage for the X-bridge; U_Y is the output voltage for the Y-bridge; E is the bridge voltage.

Figure 7   Bridge circuit mode of strain gauge for sensor

2.4   Sensing device performance and calibration test

To clarify the working performance of the designed sensing device and the relationship between the measured and actual values of the downforce. According to the above analysis and design, the prototype sensing device is shown in Figure 8. First, the working

performance of the sensing device was tested. Then, based on the 2BMG-2 tractive no-till precision planter, the sensing device was installed on the row unit to replace its original depth adjustment groove pin. The quantitative relationship between the measured X and Y values and the actual downforce of the sensing device of the gauge wheels at each depth adjustment gear was obtained by a calibration test. The models, parameters, and manufacturers of the main instruments and equipment used in the test are listed in Table 6.

a. Test results of X-direction loading

b. Test results of Y-direction loading

Figure 8　Results of test data and linear regression

Table 6　Details of test instruments and equipment

Device		Model	Parameters	Manufacturer
Universal testing machine		WDW-100E	Rangeability: 10 kN Accuracy: 1 N	Jinan Time Shijin Testing Machine Co., Ltd., China
Strain indicator		1526	Accuracy: 1 $\mu\varepsilon$	Hottinger Brüel & Kjær, Denmark
Digital multimeter		7150	Accuracy: ±0.002%	Schlumberger, Britain
DC power supply		UTP1310	Rangeability: 32 V Accuracy: 10 MV	UNI-T, China
Electronic scale		HY-601B	Rangeability: 300 kg Accuracy: 0.01 kg	Yongkang Nawei Industry and Trade Co., Ltd., China
Data acquisition device		FTNS	Frequency of sampling: 83 Hz Accuracy: ±0.1%	--

2.4.1　Performance test

1) Test method

The strain gauges of the sensing device were located according to the above analysis results, and a universal testing machine was used for loading. Loading and unloading tests were carried out in the X and Y directions of the sensing device (as shown in Figure 6), and 3 group tests were carried out in one direction. The loading locations of each group were A, B, and the midpoints of AB, and the loading forces in each test were 0, 2000, 4000, 6000, and 8000 N. A digital multimeter was used to record the voltage output under different load conditions.

2) Test results

The test data points and linear regression results are shown in Figure 8. The performance indices of the sensing device can be obtained from the test results, as listed in Table 7.
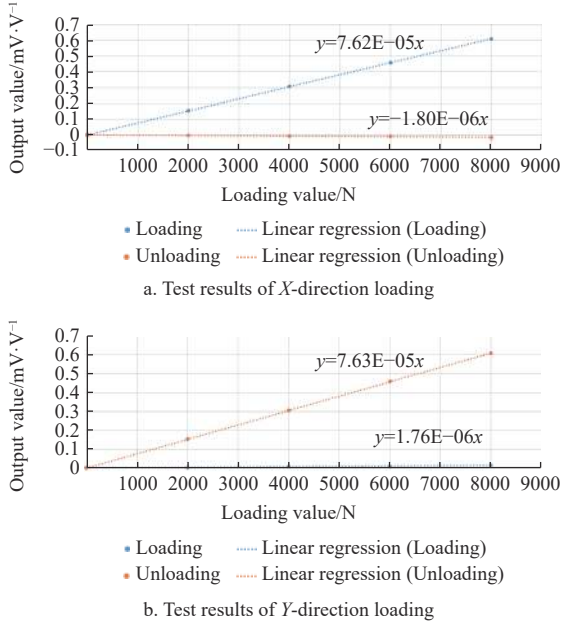
Table 7　Report of performance test

Parameters	X-direction		Y-direction	
	Loading	Unloading	Loading	Unloading
Slope	7.62E−05	−1.80E−06	7.63E−05	1.76E−06
Standard error of the slope	2.15E−07	9.57E−08	8.45E−08	2.47E−07
Sensitivity/(mV·V⁻¹)	0.6080		0.6090	
Nonlinear F·S/%	0.61		0.59	
Error of repeatability F·S/%	0.78		0.80	
Cross sensitivity F·S/%	2.52		2.50	
Lag error F·S/%	0.25		0.26	

3) Analysis of test results

Based on Table 7, the sensitivity outputs in the X- and Y-directions are 0.6080 mV/V and 0.6090 mV/V, the nonlinearities are 0.35% and 0.50%, the repeatability errors are 0.30% and 0.34%, the cross-sensitivity are 0.0253 and 0.0251, and the lag errors are 0.25% and 0.23%, respectively at full scale. Therefore, it is demonstrated that the working performance of the designed downforce sensing device meets the application requirements.

2.4.2　Calibration test

1) Calibration method

The calibration test was conducted on the 2BMG-2 tractive no-tillage precision planter, as shown in Figure 9. The test method is shown in Figure 10. Considering the sowing of maize as an example, the sowing depth was set at 50 mm for calibration, and the adjusting gear of the depth adjustment lever was set at six. First, the planter was attached to the tractor, and the sensing device was connected to the self-assembled data acquisition device by a data line. Second, the depth adjustment groove pin of the depth adjustment lever was replaced with the designed downforce measurement sensing device. Set the direction of force parallel to the depth adjustment lever as X and perpendicular to the depth adjustment lever as Y. Third, an electronic scale was put on the front fork of the forklift. Drove the forklift until the electronic scale was directly under the gauge wheels of the row unit, and then reset the initial value of the electronic balance to 0. Fourth, engage the computer to start recording data, drive the hydraulic device of the forklift truck, maintain the electronic scale rising at a constant speed, observe the changes in the electronic scale on the screen, and hold the configuration for 8-12 s each at 900, 1200, 1500, and 1800 N, while recording the test data. Finally, after the recording was completed for one test group, the electronic scale was slowly lowered until it no longer touched the gauge wheels. The measured value and actual value of the downforce were obtained through Bluetooth transmission. Each group of tests was repeated 3 times,

with then the mean value taken for regression analysis.

2) Test results and analysis

The calibration test results are listed in Table 8. According to the relevant analysis, the relationship between the actual downforce and the measured downforce is shown in Figure 11.

As shown in Figure 11, the recorded gauge wheels' actual downforce is directly proportional to the measured output downforce, and the trend is zeroed by the time intercept of the linear fitting contract. The fitting equation of the downforce calculation model is Equation (11).

$$y = 0.2332x \qquad (11)$$

where, x is the measured downforce, N; y is the gauge wheel downforce, N. The standard error of the slope of the fitting equation of the downforce calculation model is 0.008.

1. Tractor 2. Sensing device 3. Gauge wheels 4. Electronic scale 5. Front fork of the forklift

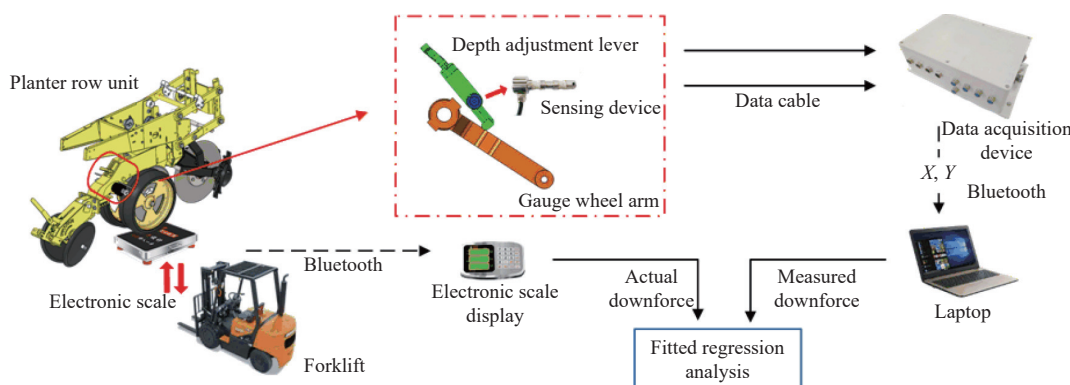Figure 9   Calibration test of sensing device

Figure 10   Calibration test method of sensing device

Table 8   Results of calibration test for the sensing device (N)

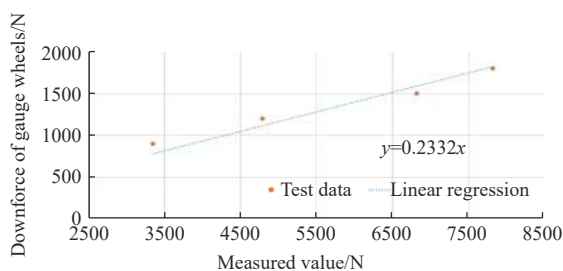| Actual downforce	X-direction	Y-direction	Measured downforce ($\sqrt{x^2 + y^2}$)
900	2016	2668	3344
1200	2803	3882	4788
1500	3923	5577	6818
1800	4482	6410	7822

Figure 11   Relationship between actual downforce and measured downforce
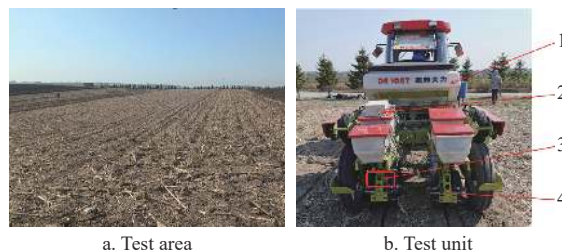
2.5   Field test

In the field, sowing will be affected by stalks, terrain, soil conditions, and other factors, so the gauge wheel downforce sensor for the row unit will constantly change. To verify the performance of the designed sensing device and understand the dynamic change in the downforce under actual working conditions, a field test was conducted in May 2023 at the Xiangyang Experimental Demonstration Base (126°55′39′′E, 45°45′48′′N), Xiangyang Township, Xiangfang District, Harbin City, Heilongjiang Province, China, as shown in Figure 12.

2.5.1   Test instruments and equipment

The main instruments and equipment in the test included a tractor, digital soil compactness tester, circular soil cutter components, data acquisition device, etc. Some of the instruments and equipment details are listed in Table 6 and Table 9.

a. Test area   b. Test unit

1. Maize no-till planter 2. Data acquisition device 3. Sensing device 4. Row unit of planter

Figure 12   Field test of downforce for no-till planter gauge wheels

Table 9   Details of field test instruments and equipment

Device		Model	Parameters	Manufacturer
	Digital soil compactness tester	TJSD-750-II	Precision: ±1%	Eijkelkamp Agrisearch Equipment Giesbeek, Neitherlands
	Circular soil cutter components	yrJ47GYN	Volume: 100 cm³	Hebei Hongyu Instrument Equipment Co., Ltd., China

2.5.2   Test conditions and method

The test plot was maize stalks free cultivated land. Applying equipment such as a digital soil compactness tester, circular soil cutter components, and drying oven, soil resistance to penetration ranging from 0.80 to 1.48 MPa at 5 cm depth and soil weight moisture content (WMC) ranging from 21.46% to 22.60% were

obtained. The downforce of the gauge wheels at different speeds of 6, 8, 10, and 12 km/h were collected. A total of 400 sample points were selected for each test data analysis and processing, and a discrete Fourier transform (DFT) was performed on the data. The transform formula is shown in Equation (12)[35].

$$X_{\text{DFT}}(f[k]) = \sum_{n=0}^{N-1} x[n] \mathrm{e}^{-i\frac{2\pi f[k]n}{f_s}} \qquad (12)$$

where, f is the sampling frequency, Hz; $f[k]$ is the discrete frequency composition of data x, $f[k] = kf_s/N$，k=0, 1, 2, …, N (N is a positive integer); $x[n]$ is a finitely sequence of N; $X_{\text{DFT}}(f[k])$ are the data after Discrete Fourier Transform.

3   Results and disscussion

According to the test, statistical analysis was carried out on the downforce of the gauge wheels, and the analysis results are listed in Table 10. Figure 13 shows the dynamic change in the downforce of the gauge wheels with time, under different speeds. Because the data signal is random and discrete, the power spectral density of the downforce at different sowing speeds can be obtained after the discrete Fourier transform and conversion of the test data, as shown in Figure 14.

1) As listed in Table 10, the downforce of the gauge wheels decreases with increasing sowing speed. The cause may be due to the existence of assembly deviation in that the parallel arms were sloped down towards the rear during the seeding operation. Accordingly, when the sowing speed increases, the forward resistance of the no-till planter row unit increases, resulting in the increase of the lifting force of the row unit, and thus the downforce of the gauge wheels is reduced.

Table 10   Statistical analysis results of the downforce of gauge wheels at different speeds

Speed/km·h⁻¹	AVG/N	COV
6	1148	0.40
8	1017	0.41
10	843	0.62
12	714	0.71

a. Time domain chart

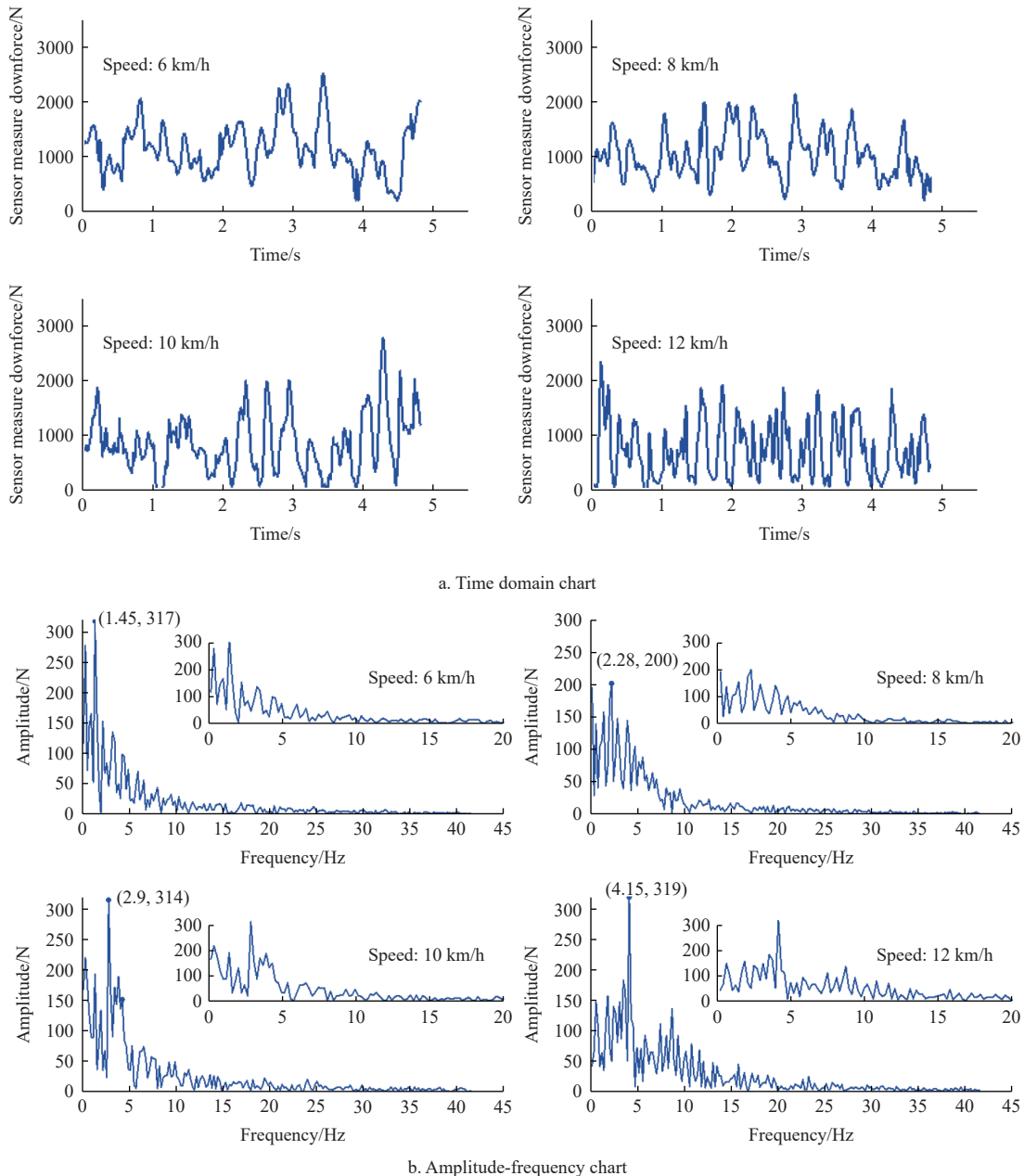b. Amplitude-frequency chart

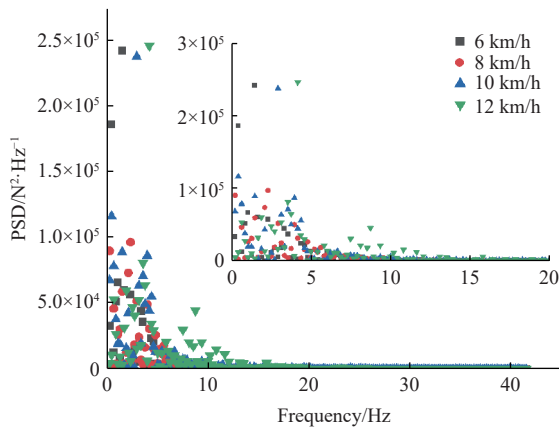Figure 13   Dynamic change of downforce for no-till planter row unit gauge wheels

Figure 14   Peak values of power spectral density of gauge wheels downforce under different speed

2) The coefficient of variation of the gauge wheel downforce increases with increasing sowing speed, indicating that the gauge wheel downforce fluctuates more violently with increasing sowing speed, as shown in Table 10. In addition, Figure 13a shows that with an increase in sowing speed, the fluctuation times of the downforce of the gauge wheels of the planter increase. When the sowing speed is greater than 10 km/h, there are many cases of the downforce of the gauge wheels of 0 N, indicating that the planter jumps and leaves the ground. Figure 13b shows that the main amplitude frequency of downforce change is the smallest at 8 km/h speed is 200 N, and the rest of the sowing speed is more than 310 N.

3) As shown in Figure 14, the main frequency of the downforce change of the gauge wheels is mostly concentrated below 5 Hz. Moreover, with increasing sowing speed, the variable high-frequency components increased. This indicates that under high sowing speed, the impact of the gauge wheel arm on the sensing device is more intense and presents a greater impact on detection accuracy.

4   Conclusions

1) The designed two-dimensional radial measurement sensing device has the characteristics of a simple structure and strong universality. Analysis shows that the ratio of the two-dimensional radial force is only related to the angle between the depth adjustment lever and the gauge wheel arm.

2) Performance and calibration tests show that the X- and Y-direction interaction of the designed and studied two-dimensional radial force sensing device is 2.52%. Under the fixed gear condition, the measured value of the sensing device has a linear relationship with the actual downforce of the gauge wheels, and the coefficient of determination of the fitting regression equation is 0.9961. The regression model has high reliability and the output signal is stable and consistent, which meets the accuracy demand of the gauge wheel downforce measurement.

3) Field tests showed that the average downforce of the gauge wheels was 1148, 1017, 843, and 713 N at 6, 8, 10, and 12 km/h, respectively, and the main frequency of the downforce signal was concentrated below 5 Hz.

Acknowledgements

[References]

[1]   Wu H C, Hu Z C, Wu F, Gu F W, Qiu T, Zhang Y H, et al. Development of automatic control system for straw smashing height adjustment device of back throwing type no-tillage planter. Transactions of the CSAE, 2019; 35(24): 1–9. (in Chinese)

[2]   Li B S, Tan Y, Chen J, Liu X X. Precise active seeding downforce control system based on fuzzy PID. Mathematical Problems in Engineering, 2020; 2020(7): 1–10.

[3]   Du Z H, He X T, Yang L, Zhang D X, Cui T, Zhong X J. Research progress on precision variable-rate seeding technology and equipment for maize. Transactions of the CSAE, 2023; 39(9): 1–16. (in Chinese)

[4]   Wang Q J, Cao X P, Wang C, Li H W, He J, Lu C Y. Research progress of No /Minimum tillage corn seeding technology and machine in Northeast Black Land of China. Transactions of the CSAM, 2021; 52(10): 1–15. (in Chinese)

[5]   Sharipov G M, Paraforos D S, Pulatov A S, Griepentrog H W. Dynamic performance of a no-till seeding assembly. Biosystems Engineering, 2017; 158: 64–75.

[6]   He J, Li H W, Chen H T, Lu C Y, Wang Q J. Research progress of conservation tillage technology and machine. Transactions of the CSAM, 2018; 49(4): 1–19. (in Chinese)

[7]   Zhang X R, Li H W, Jin H, Rasaily R G. Design and experiment of the throwing stubble and renovating the bed type no-till planter for wheat. International Agricultural Engineering Journal, 2011; 20(2): 66–70.

[8]   Poncet A M, Fulton J P, Mcdonald T P, Knappenberger T, Shaw J N. Corn emergence and yield response to row-unit depth and downforce for varying field conditions. Applied Engineering in Agriculture, 2019; 35(3): 399–408.

[9]   Drewry J L, Arriaga F J, Luck B D. Closing wheel type and row unit downforce can affect corn germination in no‐tillage production systems. Agronomy Journal, 2021; 113(5): 4037–4046.

[10]   Li M W, Xia X M, Zhu L T, Zhou R Y, Huang D Y. Intelligent sowing depth regulation system based on flex sensor and Mamdani fuzzy model for a no-till planter. Int J Agric and Biol Eng, 2021; 14(6): 145–152.

[11]   Yue L J, Wen T, Yang Q, Li Z, Li Q, Liu Y H. Effects of different sowing depths on seeding emergence of maize. Journal of Maize Sciences, 2012; 20(5): 88–93. (in Chinese)

[12]   Gao Y Y, Zhai C Y, Yang S, Zhao X G, Wang X, Zhao C J. Development of CAN based downforce and sowing depth monitoring and evaluation system for precision planter. Transactions of CSAM, 2020; 51(6): 15–28. (in Chinese)

[13]   Xue B, Zhou L M, Niu K, Zheng Y K, Bai S H, Wei L A. Sowing depth control system of wheat planter based on adaptive fuzzy PID. Transactions of CSAM, 2023; 54(S1): 93–102. (in Chinese)

[14]   Sun J Z, Zhang Y, Zhang Y T, Li P Z, Teng G F. Precision seeding compensation and positioning based on multisensors. Sensors, 2022; 22(19): 7228.

[15]   Liu W, Hu J P, Zhao X S, Pan H R, Lakhiar I A, Wang W, et al. Development and experimental analysis of a seeding quantity sensor for the precision seeding of small seeds. Sensors, 2019; 19(23): 5191.

[16]   Cay A, Kocabiyik H, May S. Development of an electro-mechanic control system for seed metering unit of single seed corn planters part II: Field performance. Computers and Electronics in Agriculture, 2018; 145: 11–17.

[17]   Maleki M R, Ramon H, De Baerdemaeker J, Mouazen A M. A study on the time response of a soil sensor based variable rate granular fertiliser applicator. Biosystems Engineering, 2008; 100(2): 160–166.

[18]   Zhou L M, Ma M, Yuan Y W, Zhang J N, Dong X, Wei C F. Design and test of fertilizer mass monitoring system based on capacitance method. Transactions of the CSAE, 2017; 33(24): 44–51. (in Chinese)

[19]   Alameen A A, Gaadi K A, Tola E. Development and performance evaluation of a control system for variable rate granular fertilizer application. Computers and Electronics in Agriculture, 2019; 160: 31–39.

[20]   Lima M C F, Krus A, Valero C, Barrientos A, del Cerro J, Roldán-Gómez J

J. Monitoring plant status and fertilization strategy through multispectral images. Sensors, 2020; 20(2): 435.

[21] Huang D Y, Zhu L T, Jia H L, Yu T T. Automatic control system of seeding depth based on piezoelectric film for no-till planter. Transactions of the CSAM, 2015; 46(4): 1–8. (in Chinese)

[22] Jia H L, Zhu L T, Huang D Y, Wang Q, Li M W, Zhao J L. Automatic control system of sowing depth for no-tillage planter based on flex sensor. Journal of Jilin University (Engineering and Technology Edition), 2019; 49(1): 166–175. (in Chinese)

[23] Zhu L T. Research on automatic control system of sowing depth for no-till planter. Master's dissertation. Changchun: Jilin Agricultural University, 2017; 51p. (in Chinese)

[24] Li Y H, Meng P X, Geng D Y, He K, Meng F H, Jiang M. Intelligent system for adjusting and controlling corn seeding depth. Transactions of CSAM, 2016; 47(S1): 62–68, 42. (in Chinese)

[25] Lynn D J, Chris N, James P L. Depth control device for planting implement. US006701857B1, 2004.

[26] Jing H, Zhang D, Wang Y, Yang L, Fan C, Zhao H, et al. Development and performance evaluation of an electro-hydraulic downforce control system for planter row unit. Computers and Electronics in Agriculture, 2020; 172: 105073.

[27] Paul R R, Elijah B G, Nathan A M, Lee E Z. Row unit for a seeding machine having active downforce control for the closing wheels. CN102726148A, 2012.

[28] Precision Planting LLC. Dynamic supplemental downforce control system for planter row units. US20180132414A1, 2018.

[29] Bai H J, Fang X F, Wang D C, Yuan Y W, Zhou L M, Niu K. Design and test of control system for seeding depth and compaction of corn precision planter. Transactions of CSAM, 2020; 51(9): 61–72. (in Chinese)

[30] Fu W Q, Dong J J, Mei H B, Gao N N, Lu C Y, Zhang J X. Design and test of maize seeding unit downforce control system. Transactions of CSAM, 2018; 49(6): 68–77. (in Chinese)

[31] Gao Y Y, Zhai C Y, Yang S, Zhao X G, Wang X, Zhao C J. Measurement method and mathematical model for the seeding downforce of planter row unit. Transactions of CSAE, 2020; 36(5): 1–9. (in Chinese)

[32] Wang Y L. Mechanics of materials 3rd ed. Beijing: China Machine Press, China, 2017; pp.50–53. (in Chinese)

[33] Sandmeyer Stell Company. Available:https://www.sandmeyersteel.com/17-4PH.html. Accessed on [2023-06-10].

[34] Al-Dahiree O S, Tokhi M O, Hadi N H, Hmoad N R, Ghazilla R A, Yap H J, et al. Design and shape optimization of strain gauge load cell for axial force measurement for test benches. Sensors, 2022; 22(19): 7508.

[35] Marchant B P. Time-frequency analysis for biosystems engineering. Biosystems Engineering, 2003; 85(3): 261–281.